Chapter 4 Laminar Boundary Layers

4. Additional Topics

a. Inlet Duct Flow
b. Rotationally Symmetrical Boundary Layers
c. Axisymmetric Boundary Layers
d. 3D Boundary Layers
e. Asymptotic Expansions
f. Unsteady Boundary Layers

Choi, J.-E., Sreedhar, M., and Stern, F., "Stokes Layers in Horizontal-Wave Outer Flows," ASME J. Fluids Eng., Vol. 118, September 1996, pp. 537 – 545.

Paterson, E.G. and Stern, F., "Computation of Unsteady Viscous Marine-Propulsor Blade Flows - Part 1: Validation and Analysis," ASME J. Fluids Eng., Vol. 119, March 1997, pp. 145 – 154.

Paterson, E.G. and Stern, F., "Computation of Unsteady Viscous Marine-Propulsor Blade Flows - Part 2: Parametric Study," ASME J. Fluids Eng, Vol. 121, March 1999, pp. 139 – 147.

Inlet Duct Flow

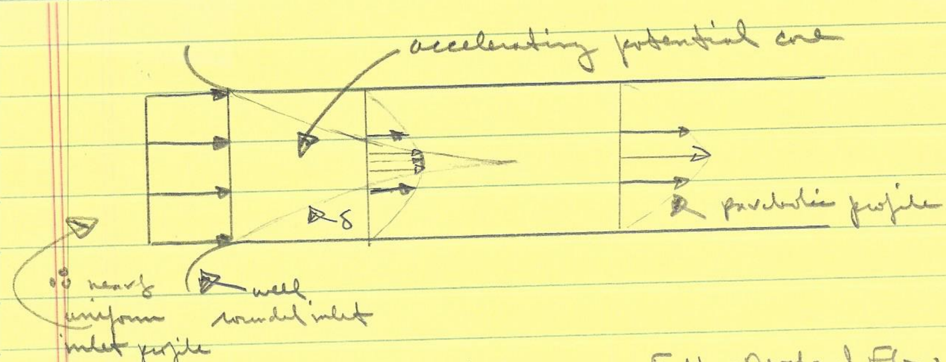

Developing Region: due to accelerating core δ is somewhat thinned | Fully-Developed Flow

$x=0$ $\qquad$ x_L

b.l. theory can predict: x_L, excess Δp over Poiseuille law, and shape of the developing profiles

$\bar{u}$ = Ave vel = Q/A

$u_p = 2\bar{u}(1 - r^2/a^2)$

excess Δp follows from cv analysis

$$(p_0 - p_x)\pi a^2 = \tau_p 2\pi a x + \int_0^x (\tau - \tau_p) 2\pi a\, dx + \rho\int_0^a (u - \bar{u}) 2\pi r\, dr$$

$$2(p_0 - p_x)/\rho\bar{u}^2 = \lambda x/D + K \qquad K = 2/3 + \int^{x/a} \frac{4(\tau - \tau_p)}{\rho\bar{u}^2}\frac{dx}{a}$$

contribution from acceleration of profile

$D = 2a$ pipe

$D = h$ channel

$$\lambda = \frac{8\tau_p}{\rho\bar{u}^2} = 64/Re_D$$

$\lambda = 96/Re_h$

Poiseuille friction coefficient

$K = K(x, Re_D, \text{duct shape (pipe or channel)})$

~ 1.31 (pipe) $.67$ (channel)

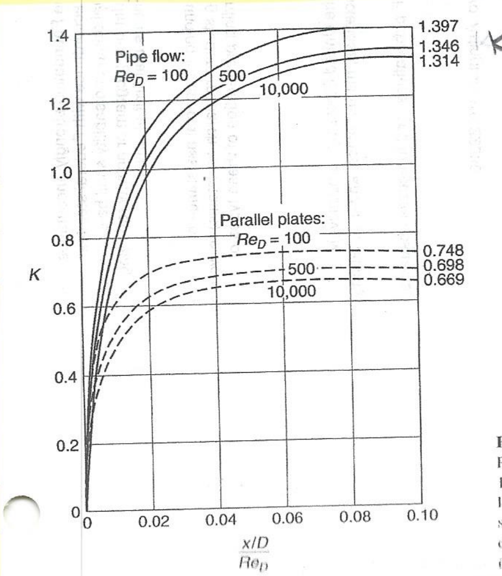

$K_\infty \big| = 1.25$ EFD

FIGURE 4-33
Pressure-drop parameter K [Eq. (4-176)] in the entrance of a duct for laminar flow. From finite-difference solutions of the full Navier–Stokes equations by Schmidt and Zeldin (1969).

TABLE 4-7
Constants to be used in Eq. (4-177)

b/a	$C_{fp}Re$	K_∞	c
	Pipe or Concentric Annulus		
0.0	16.00	1.25	0.000212
0.05	21.57	0.830	0.000050
0.10	22.34	0.784	0.000043
0.50	23.81	0.688	0.000032
0.75	23.97	0.678	0.000030
1.00	24.00	0.674	0.000029
	Rectangular Duct		
1.00	14.23	1.43	0.00029
0.50	15.55	1.28	0.00021
0.20	19.07	0.931	0.000076
0.00	24.00	0.674	0.000029
	Equilateral Triangle		
	13.33	1.69	0.00053

can also be written $\dfrac{2(p_0 - p_x)}{\rho \bar{u}^2} = C_{f,app}\, 4x/D$

apparent friction $\quad C_{f,app}\, Re = \dfrac{3.44}{\sqrt{\zeta}} + \dfrac{C_{fp}Re + K_\infty/4\zeta - 3.44/\sqrt{\zeta}}{1 + c/\zeta^2} \qquad \zeta = \dfrac{x/D}{Re_D}$

For noncircular sections use D_h & Re_{D_h}

entrance length $\quad \dfrac{x_L/D}{Re} = .08$ ie $K \to K_\infty$ upper bound

$= .01$ where BL meet lower bound but BL may set too low

$Re_D = 0$
$x_L/D = .6$ $\quad x_L/D = \dfrac{.6}{1 + .035\, Re_D} + .056\, Re_D \qquad u\big|_{CL} = .99\, u_{max}$ fully developed

creeping flow go from uniform to parabolic profile

4.9 Rotationally-Symmetric Flows

First, consider the appropriate coordinate system for the bl equations for rotationally and axisymmetric flows

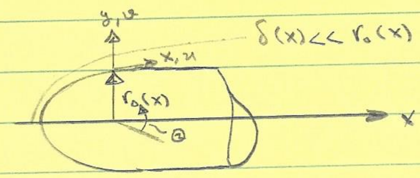

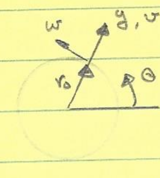

bl coord: (x, y, θ) with vel components (u, v, w)

The derivation of the rotationally symmetric bl equations involves the following steps:

(1) NS in cylindrical polar coord. (r, θ, x)

(2) transform to (x, y, θ)

(3) bl approximation

(4) rotationally symmetric flow assumption $\left(\frac{\partial}{\partial \theta} = 0\right)$

$$\frac{\partial}{\partial x}(r_0 u) + r_0 \frac{\partial v}{\partial y} = 0$$

$$\frac{\partial u}{\partial t} + u\frac{\partial u}{\partial x} + v\frac{\partial u}{\partial y} - \frac{w^2}{r_0}\frac{dr_0}{dx} = -\frac{1}{\rho}\frac{\partial p}{\partial x} + \nu\frac{\partial^2 u}{\partial y^2}$$

$$0 = \frac{\partial p}{\partial y}$$

$$\frac{\partial w}{\partial t} + u\frac{\partial w}{\partial x} + v\frac{\partial w}{\partial y} + \frac{uw}{r_0}\frac{dr_0}{dx} = \nu\frac{\partial^2 w}{\partial y^2}$$

Outside the bl, the velocity (U, W) and pressure are related via the Euler equations

$$\frac{\partial U}{\partial t} + U\frac{\partial U}{\partial x} - \frac{W^2}{r_0}\frac{dr_0}{dx} = -\frac{1}{\rho}\frac{\partial p}{\partial x}$$

$$\frac{\partial W}{\partial t} + U\frac{\partial W}{\partial x} + \frac{UW}{r_0}\frac{dr_0}{dx} = 0$$

In general, the bc are

$y=0$: $u=0$, $v = v_w(x,t)$ $w = r_0\,\Omega(t)$

↑ porous wall   ↑ rotating body

$y=\infty$: $u = U(x,t)$ $w = W(x,t)$

Some example solutions of the bl equations for rotationally symmetric flow:

(1) Rotating flow near a fixed plane
(2) Rotating sphere
(3) Conical-swirl atomizer
(4) Spinning body of revolution
(5) Decay of a swirling jet (shows interesting result that swirl decays faster than axial velocity)

A considerable amount of work has been done in recent years concerning solutions of higher-order viscous-flow equations (partially parabolic and complete NS) for swirl flows. Some of the important applications include: combustion flow (swirl is used to promote combustion through swirl-induced mixing and separation); and turbomachinery flow (see display concerning IIHR project on propeller-hull interaction)

4.91 Axisymmetric Boundary Layers ($w = 0$)

$$\frac{\partial}{\partial x}(r_0 u) + r_0 \frac{\partial v}{\partial y} = 0$$

$$u \frac{\partial u}{\partial x} + v \frac{\partial u}{\partial y} = U \frac{dU}{dx} + \nu \frac{\partial^2 u}{\partial y^2}$$

BC: $u(x,0) = 0 \quad v(x,0) = v_w(x) \quad u(x,\infty) = U(x)$

Note: only difference with 2D flow is presence of r_0 in continuity equation

Solution techniques for Axi BL:

(1) FD
(2) integral methods
(3) Similarity solution
(4) Mangler transformation (transformation to equivalent 2D flow)

We shall briefly discuss (2)–(4).

To help motivate the Mangler transformation consider the similarity solution for the flow around cones

$$U(x) = C x^n$$ potential flow past a cone of half angle θ at zero angle of attack $\theta(n)$ given in Table 4-14

Similarity transformation is

$$u/U = f'(\eta) \qquad \eta = y\left[\frac{(3+n) C x^{n-1}}{2\nu}\right]^{1/2}$$

$$\Rightarrow \quad f''' + f f'' + \frac{2n}{3+n}\left(1 - f'^2\right) = 0$$

$$f(0) = f'(0) = 0 \qquad f'(\infty) = 1$$

This is equivalent to the Falkner-Skan equation with

$$\beta_{cone} = \frac{2n}{3+n} = \beta_{wedge} = \frac{2m}{1+m}$$

ie,

$$m_{wedge} = 1/3\, n_{cone}$$

Thus, the cone flow $U = Cx^n$ has similar properties as the wedge flow $U = c' x^{n/3}$, and the Falkner-Skan equation determines both.

4.92 Mangler Transformation

The cone-flow similarity solution suggests the possibility of transforming the Axi bl equations to an equivalent 2D flow. This was, in fact, accomplished by Mangler as follows:

let $$x' = \frac{1}{L^2}\int_0^x r_0^2\,dx \qquad y' = r_0 y / L$$

$$u' = u \qquad U'(x') = U(x) \qquad v' = \frac{L}{r_0}\left(v + \frac{y u}{r_0}\frac{dr_0}{dx}\right)$$

in which L = reference length. With this transformation the Axi bl equations reduce to

$$\frac{\partial u'}{\partial x'} + \frac{\partial v'}{\partial y'} = 0$$

$$u'\frac{\partial u'}{\partial x} + v'\frac{\partial u'}{\partial y} = U'\frac{dU'}{dx} + \nu\frac{\partial^2 u'}{\partial y'^2}$$

Note: (1) All 2D methods discussed previously are applicable

(2) $U'(x')$ does not bear any resemblance to $U(x)$ and may present difficulties in obtaining solutions

Three dimensional boundary layers

$$u_x + v_y + w_z = 0$$

$$u u_x + v u_y + w u_z = -p_x/\rho + \nu u_{yy}$$

$$u w_x + v w_y + w w_z = -p_z/\rho + \nu w_{yy}$$

Flow driven by both p_x & p_z

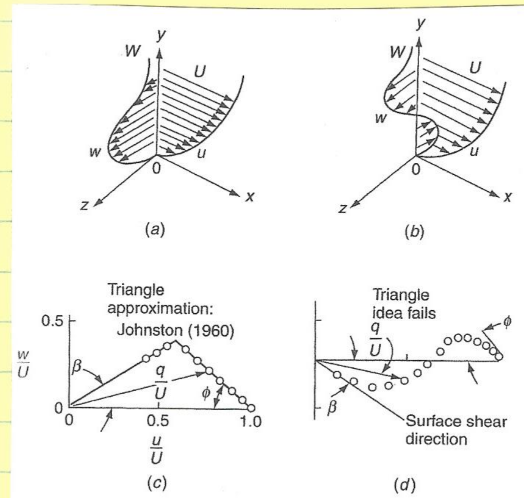

$$\tan\beta = \left.\frac{\tau_{zy}}{\tau_{xy}}\right|_{wall}$$

FIGURE 4-42
Unidirectional and bidirectional skewing in three-dimensional pressure-driven boundary layers: (*a*) unidirectional skewing; (*b*) bidirectional skewing; (*c*) unidirectional hodograph; (*d*) bidirectional hodograph.

Complex crossflow such as (b): death of 3D integral methods

Motivated 3D differential BL methods

Thick BL & separation led to rapid extension differential methods to modern CFD: RANS, HRLES, LES, DNS!

Boundary Layer with constant transverse pressure gradient: flat plate BL with parabolic free stream

Flat plate with LE at $x=0$ & inflow at angle θ_0

For $x>0$ & $y \to \infty$

$$u = u_e = \text{constant} \qquad p_x = 0$$

$$w = w_e = u_e(a+bx) \qquad -p_z/\rho = u_e w_{e_x} = u_e^2 b$$

External flow $\underline{\omega} = \omega_y \hat{j}$ $\qquad$ b = magnitude transverse p_z

$$\omega_y = -\frac{\partial w}{\partial x} = -u_e b$$

For $b=0$ $\theta = \theta_0 = \tan^{-1}\frac{w_e}{u_e} = \tan^{-1} a$, which shows the effect of sweep on Blasius BL

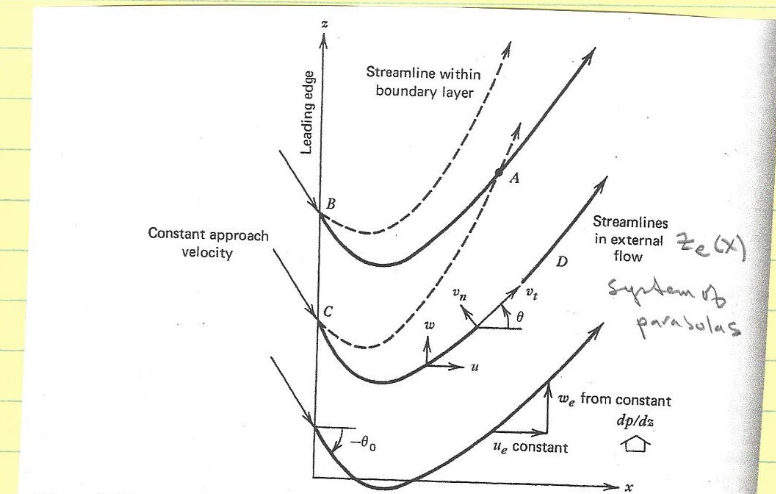

Figure 20.30 Plan view of the boundary layer on a plate with a constant transverse pressure gradient.

$$\frac{dz_e}{dx} = \frac{w_e}{u_e} = a + bx$$

$$z_e = ax + \tfrac{1}{2}bx^2 + c$$

$$c = \text{constant} = z_e\big|_{LE}$$

Concept of region of influence: particles that pass through C influence region CAD. 3D BL methods must account for spreading lateral influence

BL equations:

$$u_x + v_y = 0$$

$$u u_x + v u_y = \nu u_{yy}$$

$$u w_x + v w_y = S u_0^2 + \nu w_{yy}$$

continuity & x-momentum $\neq f(w)$ = Blasius BL problem

$$u/u_e = f'(\eta) \qquad \eta = y\sqrt{u_e/\nu x}$$

$f(\eta)$ solution Blasius equation: $ff'' + 2f''' = 0$

Sweep independence principle: u, v solved independent w

Assume: $$w/u_e = \underbrace{\frac{w_e(x)}{u_e} f'(\eta)} + S x h(\eta)$$

Blasius component scaled to match $w_e(x)$

Substitution in w-momentum equation

$$h'' + \tfrac{1}{2} f h' - f'h + 1 - f'^2 = 0$$

$$h(0) = h(\infty) = 0$$

} Similarly Blasius equation solved numerically

Solutions use normal and tangential coordinates to outer flow and normalized with outer flow velocity magnitude

$$V_\infty = [u_e^2 + w_e^2]^{1/2}$$

$v_t/V_\infty = f'(\eta) + \frac{1}{2}\sin 2\theta(\tan\theta - \tan\theta_0)\,h(\eta)$

$v_n/V_\infty = \frac{1}{2}\cos^2\theta(\tan\theta - \tan\theta_0)\,h(\eta)$

θ = local inviscid ψ angle $\tan^{-1} w_e/u_e$

(1) flat plate with sweep angle $\theta = \theta_0$ & $s=0$

Blasius profile & no secondary flow ie $v_n = 0$

If ψ_e coincides with the surface geodesic curve $\psi_{BL} = \psi_e$ & no secondary flow

Geodesic curve: curve whose tangent vectors remain parallel if they are transported along it

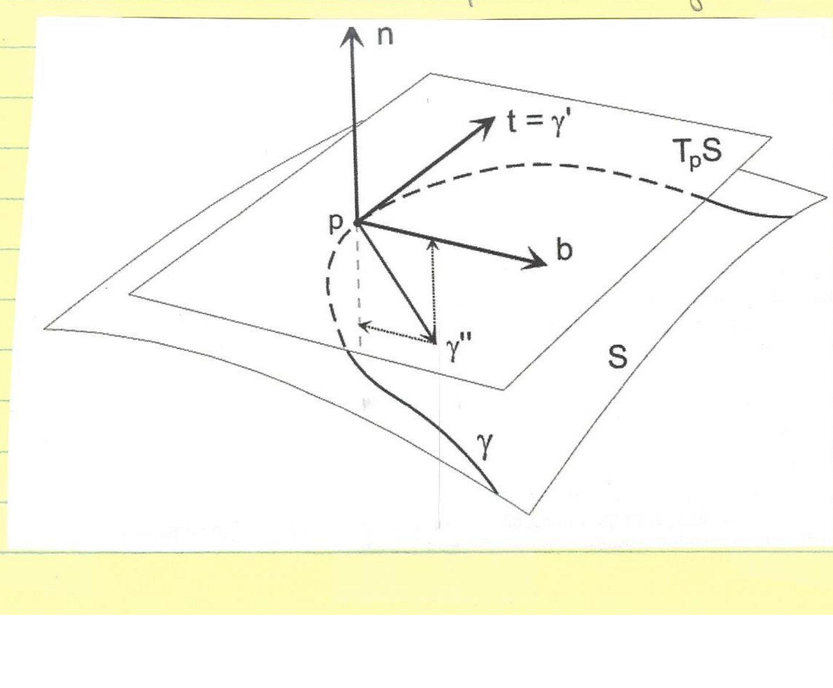

(2) $\theta \neq \theta_0$ & $b \neq 0$

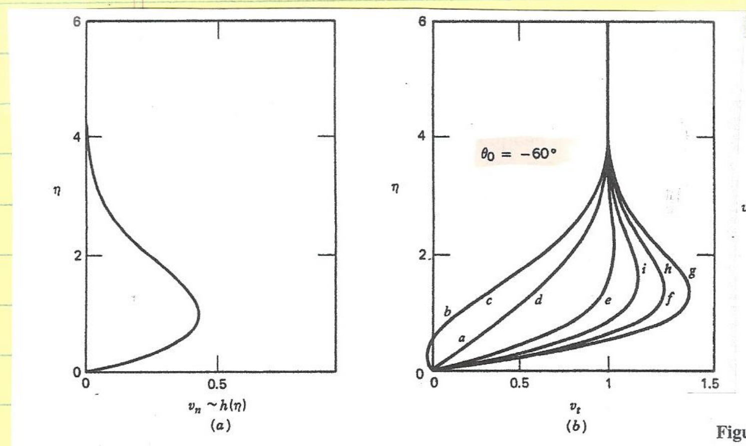

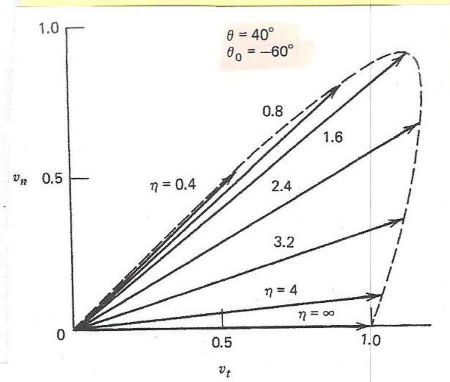

Figure 20.32 Polar diagram of velocity profile with overshoot.

Figure 20.31 Typical velocity profiles: (*a*) transverse profiles $h(\eta)$; and (*b*) tangential profiles for various flow angles: $a, \theta = -60°$; $b, \theta = -40°$; $c, \theta = -20°$ (same curve as b); $d, \theta = 0°$ (same as a); $e, \theta = 20°$; $f, \theta = 40°$; $g, \theta = 60°$; $h, \theta = 80°$ (same as f); $i, \theta = 90°$.

θ		v_n not shown since $\propto h(\eta)$
−60	a	Blasius
−40	b	} $v_t < 0$ near $\eta = 0$, but not reverse flow
−20	c	v_n large such that
0 = a	d	Blasius — flow > 0 in x direction
20	e	
40	f	} v_t exhibits overshoot in upper BL
60	g	occurs frequently in 3D BL
80 = f	h	in this region (similar as Stokes 2nd
90	i	problem for oscillating outer flow) net

transverse viscous force same direction pressure force. Viscous force dies out at large η

Note: flow never actually separates

$$z_s = ax + \tfrac{1}{2} b x^2 \left[1 + \frac{h'(0)}{f''(0)}\right] + C_0$$

also parabolas and differ z_e by $1 + \frac{h'(0)}{f''(0)} \approx 1 + \frac{1}{3}$